

# Phonon signatures of multiferroicity in $\text{TbMn}_2\text{O}_5$

R. Valdés Aguilar,<sup>1</sup> A. B. Sushkov,<sup>1</sup> S. Park,<sup>2</sup> S-W. Cheong,<sup>2</sup> and H. D. Drew<sup>1</sup>

<sup>1</sup>*Materials Research Science and Engineering Center,  
University of Maryland, College Park, Maryland 20742*

<sup>2</sup>*Rutgers Center for Emergent Materials and Department of Physics and Astronomy,  
Rutgers University, Piscataway, New Jersey 08854*

The infrared (IR) active phonons in multiferroic  $\text{TbMn}_2\text{O}_5$  are studied as a function of temperature. Most of the symmetry allowed IR modes polarized along the  $a$  and  $b$  crystal axes are observed and the behavior of several  $b$  polarized phonons is correlated with the magnetic and ferroelectric transitions. A high frequency  $b$  polarized phonon only Raman allowed in the paraelectric phase becomes IR active at the ferroelectric transition. The IR strength of this mode is proportional to the square of the ferroelectric order parameter and gives a sensitive measure of the symmetry lowering lattice distortions in the ferroelectric phase.

PACS numbers: 78.30.-j 63.20.Ls 75.50.Ee

## I. INTRODUCTION

Materials that exhibit simultaneously (anti)-ferromagnetic, (anti)-ferroelectric or (anti)-ferroelastic degrees of freedom, the so called multiferroics, have become of increasing interest because they offer great possibilities for applications in multifunctional devices. These applications are specially based on the power to control the magnetic state by electric fields and the ferroelectric state by magnetic fields, this type of materials being the magnetoelectrics, a subclass of the multiferroics<sup>1,2,3,4</sup>. Moreover, the understanding of the basic mechanism that allows this behavior is crucial in the development of the devices that make use of these characteristics.

The interplay of these degrees of freedom has been demonstrated recently in several multiferroic materials such as  $Re\text{Mn}_2\text{O}_5$  where  $Re$  is Eu, Gd, Tb, Dy, Ho and Y<sup>5,6,7,8</sup> as well as in  $\text{TbMnO}_3$ <sup>9</sup> and  $\text{Ni}_3\text{V}_2\text{O}_8$ <sup>10</sup>. Fundamental questions as to the nature and characteristics of the coupling of the magnetic and ferroelectric orders remain unanswered. Phenomenological approaches<sup>11,12</sup> based on the Landau theory of phase transitions have been used to relate the symmetry of the spin order with the appearance of ferroelectricity. The basic conclusion of these proposals is that the non-collinearity of the spin system is crucial in the development of ferroelectric order. More microscopic studies<sup>13,14</sup> have also pointed to the importance of non-collinearity of the spin system.

The antiferromagnetic manganese oxide  $\text{TbMn}_2\text{O}_5$  (orthorhombic space group Pbam # 55,  $Z = 4$ ) is a multiferroic with non-collinear magnetic order<sup>15</sup> that shows a strong magnetoelectric coupling effect<sup>6</sup>: an applied magnetic field along the  $a$  axis changes the sign of the electrical polarization present along the  $b$  axis. The behavior of the dielectric constant  $\epsilon$  along  $b$  (see figure 1 in Hur, et al<sup>6</sup>) at low frequency, where distinct phase transitions are observed, is the following: at the Néel temperature  $T_N \approx 42$  K no anomalies are present in  $\epsilon$ . There is a paraelectric to ferroelectric phase transition at  $T_C \approx 38$  K ev-

ident by a peak in the dielectric constant. The magnetic order then locks in to a commensurate structure (CM) with wave vector (1/2,0,1/4). At  $T \approx 24$  K the magnetic order transforms into an incommensurate structure (ICM) with a step-like feature in  $\epsilon$ ; this anomaly is also accompanied by hysteresis<sup>6</sup>. We note that the dielectric constants along the  $a$  and  $c$  axis show no significant effects at these phase transitions.

In  $\text{EuMn}_2\text{O}_5$  Polyakov, et al<sup>16</sup> found displacements of the  $\text{Mn}^{3+}$  ion along the  $a$  axis at the ferroelectric transition. They suggested that this behavior leads to a change in symmetry from the space group Pbam to the non-centrosymmetric group  $P2_1am$  (# 26). In similar, work on the compound  $\text{YMn}_2\text{O}_5$ <sup>17</sup>, Kagomiya, et al proposed similar displacements at the ferroelectric transition. The displacements reported are very small ( $\approx 0.007$  Å), which hints to a different origin of the ferroelectricity when compared to the typical proper ferroelectrics. Other structural works<sup>15,18,19</sup> have not reported any signature of significant atomic displacements at the ferroelectric phase transition in this family of compounds. Moreover, Mihailova, et al<sup>20</sup> reported a Raman study in  $\text{HoMn}_2\text{O}_5$ ,  $\text{TbMn}_2\text{O}_5$  and García-Flores, et al<sup>21</sup> in  $\text{BiMn}_2\text{O}_5$ ,  $\text{EuMn}_2\text{O}_5$  and  $\text{DyMn}_2\text{O}_5$  as a function of temperature and found no evidence of anomalous behavior of the Raman active phonons at the ferroelectric transition temperature. Nevertheless, the existence of a macroscopic dipole moment is evidence of the lack of inversion symmetry in the crystal, and motivates the study of the dynamics of the lattice to look for further information about the change in symmetry.

In this report we present a study of the temperature dependent infrared (IR) phonon spectra of the multiferroic  $\text{TbMn}_2\text{O}_5$ . The most interesting feature we find is the appearance of an IR inactive phonon activated at the ferroelectric transition with  $E \parallel b$ . This indicates that one IR forbidden mode (Raman or silent) in the paraelectric phase acquires an electric-dipole moment due to the static displacement associated with the ferroelectricity. We identify this phonon with a Raman Mn-O stretching mode, which accounts for its sensitivity to

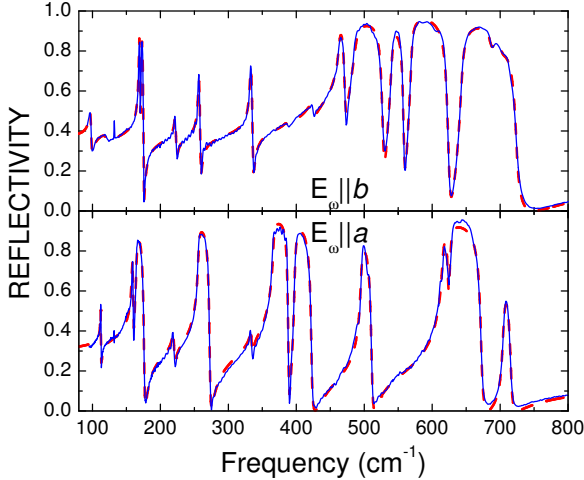


FIG. 1: (Color Online). Experimental (solid line) and fit (dashed line) at  $T = 7$  K phonon spectra in  $\text{TbMn}_2\text{O}_5$ . (Top)  $b$  axis reflectivity; (Bottom)  $a$  axis reflectivity. See the text for details.

the macroscopic polarization possibly induced by the Mn spin system.<sup>11,19</sup>

## II. EXPERIMENTAL RESULTS

Single crystals of  $\text{TbMn}_2\text{O}_5$  were grown using  $\text{B}_2\text{O}_3/\text{PbO}/\text{PbF}_2$  flux in a Pt crucible. The flux was held at  $1,280$  °C for 15 hours and slowly cooled down to  $950$  °C at a rate of  $1$  °C per hour. Crystals grew in the form of black platelets as well as cubes with a typical size of  $10$  mm<sup>3</sup>. Normal incidence reflection spectra were taken with a Bomem Fourier Transform Spectrometer DA3.02. Light was polarized along the  $a$  and  $b$  crystal axes in the frequency range  $8-800$  cm<sup>-1</sup> ( $\approx 1-100$  meV) and in the temperature range  $7$  to  $300$  K. Sample was kept in vacuum in a continuous He flow cryostat with optical access windows. The factor group analysis based on structural data by Alonso, et al<sup>22</sup> gives the following IR active vibrational modes at the  $\Gamma$  point:  $\Gamma_{IR} = 8B_{1u}E||z + 14B_{2u}E||y + 14B_{3u}E||x$  consistent with a previous report<sup>20</sup>.

Figure 1 shows the spectra at  $T = 7$  K. Twelve of the 14 IR active phonons in the  $a$  polarization were reliably observed, whereas all 14 phonons polarized along  $b$  are present in the spectrum. The reflectivity spectra was fitted with the sum of Lorentzian form of the model dielectric function  $\varepsilon$  given by:

$$\varepsilon(\omega) = \varepsilon_\infty + \sum_{i=1}^N \frac{S_i \omega_{oi}^2}{\omega_{oi}^2 - \omega^2 - i\gamma_i \omega} \quad (1)$$

where  $\varepsilon_\infty$  is the dielectric constant at high frequency and the phonon parameters ( $\omega_o$ ,  $S$  and  $\gamma$ ) are extracted as

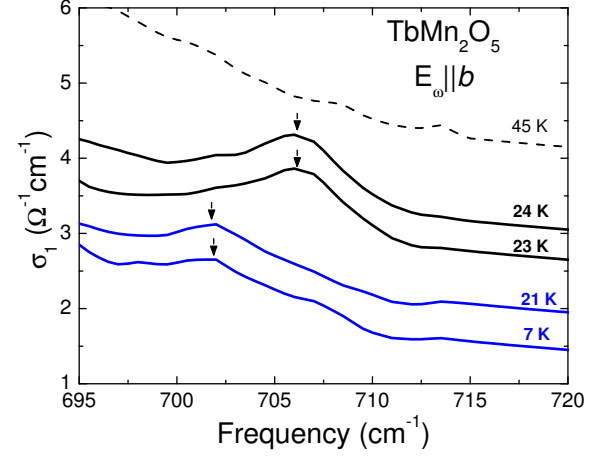


FIG. 2: (Color Online). Conductivity of the newly activated phonon (manually shifted plots). In black is the CM phase. In bold blue is the temperature range below  $\text{CM} \rightarrow \text{ICM}$  transition. Arrows indicate the position of the phonon frequency fit.

functions of temperature and are displayed in table I. The result of the fitting is also shown in figure 1 and it can be seen that it is almost indistinguishable from the data indicating the weakness of higher order phonon processes.

Figure 2 is a plot of the optical conductivity in a narrow frequency range around  $700$  cm<sup>-1</sup> for several temperatures with light polarized along the  $b$  axis (parallel to the macroscopic polarization). We observe that a fea-

TABLE I: Oscillator parameters at  $T_1 = 7$  K and  $T_2 = 45$  K in  $\text{TbMn}_2\text{O}_5$ .  $a$ ,  $b$  are the crystal axes.

$\omega_o(\text{cm}^{-1})$				$S$				$\gamma(\text{cm}^{-1})$			
$a$		$b$		$a$		$b$		$a$		$b$	
$T_1$	$T_2$	$T_1$	$T_2$	$T_1$	$T_2$	$T_1$	$T_2$	$T_1$	$T_2$	$T_1$	$T_2$
111.9	111.7	97.2	96.4	0.59	0.66	0.42	0.38	1.9	2	3.3	3.7
157.5	157.3	168.9	168.6	2.89	3.88	0.46	0.43	3.3	2.6	1	1.1
164.2	163.8	171.9	171.5	1.68	2.02	0.30	0.35	0.9	0.3	1.4	1.5
218.5	217.4	222.2	221.9	0.30	0.69	0.11	0.11	4.7	8.9	2.4	2.9
254.8	253.2	256.8	256.6	1.88	2.56	0.17	0.18	3.1	1.5	2.1	2
333.1	332.4	333.4	332.7	0.09	0.15	0.17	0.17	2.7	2.6	2.7	2.7
364.9	362.8	386	385.5	2.02	2.75	0.02	0.01	3.9	1	3.5	4
397.6	396.5	422.3	422.3	0.38	0.46	0.28	0.28	4.6	3.2	4	3.5
494.8	493.9	453.2	459.3	0.45	0.59	3.43	3.56	5.3	3.7	18.4	6.7
613.5	611.3	481.8	483	0.71	1.11	1.03	2.6	9	5.4	4.4	3.3
627.5	625.9	538.2	537.6	0.23	0.14	0.25	0.51	8.4	4.2	7.3	7.1
704.2	701.4	567.3	568.4	0.05	0.04	0.27	0.57	3.3	4.5	5.1	7.9
—	—	636.6	637.2	—	—	0.10	0.23	—	—	10.7	9.3
—	—	688.2	686.9	—	—	0.003	0.003	—	—	9.5	6
—	—	703 <sup>a</sup>	—	—	—	0.001	—	—	—	26	—
—	—	120.4 <sup>b</sup>	119.5	—	—	0.12	0.10	—	—	5.7	6.4

<sup>a</sup>Previously IR inactive

<sup>b</sup>Crystal field excitation fitted as electric dipole active

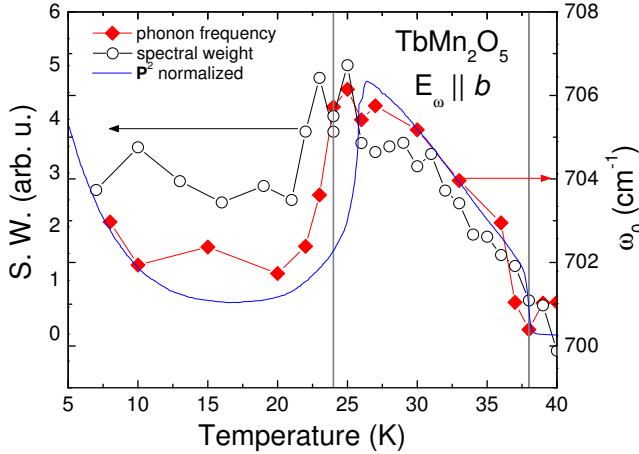


FIG. 3: (Color Online). Spectral weight and frequency of the activated phonon. The continuous line is the measured polarization squared. The spectral weight and frequency follow closely the behavior of the polarization in the CM phase.

ture not present at 45 K appears at the low T phases. The temperature dependence of the spectral weight and frequency of this feature is plotted in figure 3 where we see the spectral weight starting to appear at 38 K. The spectral weight of this phonon increases and its frequency shifts, both continuously, as we lower the temperature. At 24 K the spectral weight and frequency change both abruptly and show hysteresis. The behavior of this feature is correlated with the second order FE transition at 38 K and the first order CM  $\rightarrow$  ICM transition at 24 K in this compound.

On very general grounds we can relate the appearance and behavior of this phonon to these underlying phase transitions. Since the lattice distortions  $\delta u$  associated with these phase transitions are very small we can expand the spectral weight and frequency shifts in powers of  $\delta u$ . The quadratic term is the first non-zero term in this expansion that can describe the spectral weight change or frequency shift. Similarly, the order parameters associated with the new phases are proportional to  $\delta u$  so that  $\mathbf{P} \approx \delta u$ . As a result we expect that the spectral weight behavior and frequency shift should be  $S, \Delta\omega \approx (\delta u)^2 \approx \mathbf{P}^2$ . This is the behavior observed as can be seen in figure 3a where we have plotted  $\mathbf{P}^2$  with the phonon data. At low temperatures ( $T < 10$  K) where the Tb moment orders, the phonon data deviates from  $\mathbf{P}^2$  suggesting that it is the Mn and oxygen ion displacements that dominate the dynamics of this high frequency phonon. In this multiferroic material it is proposed<sup>11,19</sup> that the primary order is magnetic and the non-collinear magnetism drives the FE order. Therefore it would be expected that  $\mathbf{P} \approx N$ , where  $N$  is the magnetic order parameter. Data on temperature dependence of the magnetic order parameter could not be found for this material to test this prediction.

The possible scenarios for the appearance of a new phonon are: (1) zone folding of the phonon dispersion (since the magnetic order corresponds to a lock in ICM  $\rightarrow$  CM transition with  $\mathbf{k} = (1/2, 0, 1/4)$ ), and (2) activation of IR-inactive phonons at this transition due to the loss of inversion symmetry. We performed a shell model calculation for the phonon dispersion and this shows that the dispersion of the high frequency phonon is negative so that no zone-folded mode can give the high frequency of this phonon. We therefore conclude that this phonon is a previously IR inactive phonon that acquires electric dipole moment at the FE transition.

In a ferroelectric phase transition, where inversion symmetry is lost, symmetry considerations dictate that phonons that were not IR active in the paraelectric phase can become IR active in the FE phase. This is the case in  $\text{TbMn}_2\text{O}_5$ , where the low T phase has mixed IR and Raman phonons. In this low T phase the phonons of the high T symmetry group split as shown in table II. This splitting was obtained by considering what symmetry operation is maintained in both phases and then assign spectral activity according to the experimental observations. Consistency with the laboratory frame ( $x \rightarrow a, y \rightarrow b, z \rightarrow c$ ) is applied as well. From the reports by Mihailova, et al.<sup>20</sup> and García-Flores, et al.<sup>21</sup> we learn that a  $A_g$  mode at frequency  $\approx 700 \text{ cm}^{-1}$  exists in all the  $\text{ReMn}_2\text{O}_5$  materials whose Raman phonons have been reported. We note as well that these reports do not resolve any IR phonons becoming Raman active at the FE phase transition. We conclude that this high frequency  $A_g$  Raman phonon is the mode we observe that acquires IR activity in the FE phase. Further experimental confirmation is needed to make a definitive identification.

Only a few other phonons show correlations with the low temperature phase transitions. The phonons polarized along the  $a$  axis do not show any significant anomalies in this temperature range. This is as expected since the dielectric function along this axis is featureless. On the other hand, the behavior of some of the phonons with

TABLE II: Irreducible representation splitting at the FE phase transition. S. A. = Spectral Activity (R = Raman active, IR = Infrared Active).

# 55 S. A.	# 55 irreps	# 26 irreps	#26 S. A. <sup>a</sup>
R	$A_g$	$A_1$	IR (y) & R
R	$B_{1g}$	$B_2$	IR (x) & R
R	$B_{2g}$	$A_2$	R
R	$B_{3g}$	$B_1$	IR (z) & R
Silent	$A_u$	$A_2$	R
IR(z)	$B_{1u}$	$B_1$	IR (z) & R
IR(y)	$B_{2u}$	$A_1$	IR (y) & R
IR(x)	$B_{3u}$	$B_2$	IR (x) & R

<sup>a</sup>Note that in this column x, y, z correspond to the high temperature system of coordinates  $a, b, c$  and differ from what is found in the character table.

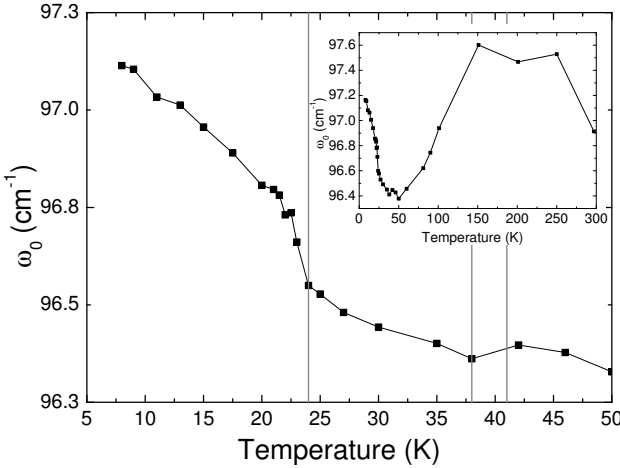


FIG. 4: Temperature dependence of the  $b$  axis Tb phonon frequency. In the inset the full temperature range is plotted. We observe softening below  $\approx 150$  K and then hardening back when it becomes AFM. There is also additional hardening below the 23 K transition.

dipole moment along  $b$  is non-trivial. The low frequency phonon with frequency  $\approx 96 \text{ cm}^{-1}$ , identified primarily with movement of the Tb ions, has a temperature dependence that correlates with the low temperature CM  $\rightarrow$  ICM magnetic transition. In figure 4 the frequency of this phonon is plotted versus temperature and we observe an increase in the frequency around 24 K. This effect is thought to be a manifestation of the coupling of this phonon to a magnon as is discussed by Katsura, et al<sup>23</sup>. Further experimental results on this effect will be presented elsewhere<sup>24</sup>.

Surprisingly several phonons show interesting temperature dependence for  $T$  above  $T_N$ . The inset in figure 4 shows the full temperature dependence of the frequency of the  $b$  axis phonon. The anomalous softening in the temperature range of 150 K to 50 K demonstrates additional effects in the dynamics of the lattice. In figure 5 the behavior of the spectral weight of two oxygen phonons polarized in the  $a$  and  $b$  axes, with frequencies of 704 and  $689 \text{ cm}^{-1}$  respectively, seems complementary: the  $a$  phonon gains spectral weight while the  $b$  phonon loses it as the temperature is lowered. This effect is present in the full temperature range from 300 K to 7 K, while for the rest of the phonons the spectral weight is only changed significantly around the various transition temperatures. The fact that these modes gain or lose so much spectral weight (10 and 6-fold respectively) in a large temperature scale also demonstrates some higher energy energy scale in this system. These effects (the anomalous softening and the dramatic changes in spectral weight) are not understood at present. However, one interesting possibility is that they are of magnetic character. Recent high temperature susceptibility measurements<sup>21</sup> in  $\text{BiMn}_2\text{O}_5$  has shown evidence for spin frustrated behavior from devia-

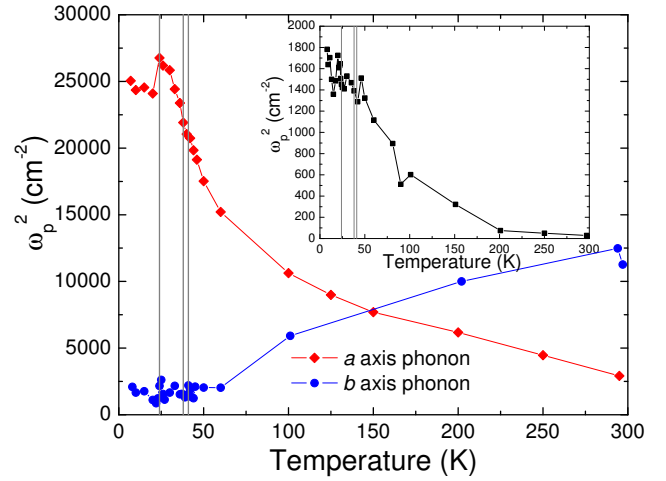


FIG. 5: (Color Online). Temperature dependence of the spectral weight of 2 oxygen dominated phonons. The net gain (loss) is 10 (6) fold. Inset shows the temperature dependence of the intensity of one of the  $\text{Tb}^{3+}$  crystal field transitions.

tions from Curie law with a Weiss temperature of  $\approx 250$  K. Another possibility is that this phonon features are consequence of structural anomalies at higher temperatures as is suggested by dielectric measurements above the Néel temperature<sup>25</sup>.

Finally the inset of figure 5 shows the temperature dependence of the intensity of a feature observed at  $120 \text{ cm}^{-1}$ . This is identified as a crystal field level of the  $\text{Tb}^{3+}$  ion<sup>26</sup>. This transition has electric dipole character as is seen from the form of the reflectivity curve (see fig. 1) as well as the fact that the spectral weight (see table I) is comparable to the IR active phonons (magnetic dipole transitions are usually much weaker than electric dipole transitions). This conclusion is supported as well by the shell model calculation that shows the 3 lowest phonon excitations being the Tb-dominated phonon (at  $\approx 100 \text{ cm}^{-1}$ ) and then a doublet (at  $\approx 170 \text{ cm}^{-1}$ ). Furthermore, the observed temperature dependence of the intensity is common for the f-level crystal field transitions in the rare earth elements<sup>27</sup>. Several other weaker absorption features are observed in transmission at lower frequencies.

### III. CONCLUSIONS

We have measured the IR phonon spectra in  $\text{TbMn}_2\text{O}_5$  along the  $a$  and  $b$  axes and have observed most of the symmetry allowed modes. The majority of the phonons do not show significant correlations to the FE and AFM phase transitions of the system. However several phonons exhibit interesting correlations to the ferroelectricity of this material. We have found a signature of the loss of inversion symmetry in the FE phase by the appearance of a IR phonon below  $T_c$  that was only Raman active in

the paraelectric phase. The strength of this mode is proportional to the square of the FE order parameter and gives a sensitive measure of the symmetry lowering lattice distortions in the ferroelectric phase. In addition, the lowest frequency phonon (along *b*) displays hardening in the CM  $\rightarrow$  ICM transition possibly due to the coupling with the spin system<sup>23</sup>; 2 modes (along *a* and *b*) have dramatic changes in their spectral weight over a wide temperature range possibly because of structural anomalies at higher temperatures or because of frustration effects in the spin system. We have also identified a

electric dipole active crystal field transition of the Tb<sup>3+</sup> ion in the phonon frequency range.

#### IV. ACKNOWLEDGEMENTS

We thank G-W. Chern, D.I. Khomskii, S. Jandl, J. Simpson and O. Tchernyshyov for useful discussions. This work was supported by the National Science Foundation MRSEC under Grant No. DMR-0520471.

- 
- <sup>1</sup> N. A. Hill and A. Filippetti, *J. Mag. Mag. Mat.* **242-245**, 976 (2002).
- <sup>2</sup> M. Fiebig, T. Lottermoser, T. Lonkai, A. V. Goltsev, and R. V. Pisarev, *J. Mag. Mag. Mat.* **290-291**, 883 (2005).
- <sup>3</sup> W. Prellier, M. P. Singh, and P. Murugavel, *J. Phys. Condens. Matter* **17**, R803 (2005).
- <sup>4</sup> C. Binek and B. Doudin, *J. Phys. Condens. Matter* **17**, L39 (2005).
- <sup>5</sup> Y. F. Popov, A. M. Kadomtseva, S. S. Krotov, G. P. Vorob'ev, and M. M. Lukina, *Ferroelectrics* **279**, 147 (2002).
- <sup>6</sup> N. Hur, S. Park, P. Sharma, J. Ahn, S. Guha, and S.-W. Cheong, *Nature* **429**, 392 (2004).
- <sup>7</sup> N. Hur, S. Park, P. A. Sharma, S. Guha, and S.-W. Cheong, *Phys. Rev. Lett.* **93**, 107207 (2004).
- <sup>8</sup> E. Golovenchits and V. Sanina, *J. Phys. Condens. Matter* **16**, 4325 (2004).
- <sup>9</sup> T. Kimura, T. Goto, H. Shintani, K. Ishizaka, T. Arima, and Y. Tokura, *Nature* **426**, 55 (2003).
- <sup>10</sup> G. Lawes, A. B. Harris, T. Kimura, N. Rogado, R. J. Cava, A. Aharony, O. Entin-Wohlman, T. Yildrim, M. Kenzelmann, C. Broholm, et al., *Phys. Rev. Lett.* **95**, 087205 (2005).
- <sup>11</sup> M. Mostovoy, *Phys. Rev. Lett.* **96**, 067601 (2006).
- <sup>12</sup> A. B. Harris (2005), CondMat/0508730.
- <sup>13</sup> H. Katsura, N. Nagaosa, and A. Balatsky, *Phys. Rev. Lett.* **95**, 057205 (2005).
- <sup>14</sup> I. Sergienko and E. Dagotto, *Phys. Rev. B* **73**, 094434 (2006).
- <sup>15</sup> L. Chapon, G. Blake, M. Gutmann, S. Park, N. Hur, P. Radaelli, and S.-W. Cheong, *Phys. Rev. Lett.* **93**, 177402 (2005).
- <sup>16</sup> V. Polyakov, V. Plakhty, M. Bonnet, P. Burlet, L.-P. Regnault, S. Gravilov, I. Zobkalo, and O. Smirnov, *Physica B* **297**, 208 (2001).
- <sup>17</sup> I. Kagomiya, S. Matsumoto, K. Kohn, Y. Fukuda, T. Shoubu, H. Kimura, Y. Noda, and N. Ikeda, *Ferroelectrics* **286**, 167 (2002).
- <sup>18</sup> G. Blake, L. Chapon, P. Radaelli, S. Park, N. Hur, S.-W. Cheong, and J. Rodríguez-Carvajal, *Phys. Rev. B* **71**, 214402 (2005).
- <sup>19</sup> L. Chapon, P. Radaelli, G. Blake, S. Park, and S.-W. Cheong, *Phys. Rev. Lett.* **96**, 097601 (2006).
- <sup>20</sup> B. Mihailova, M. Gospodinov, B. Guttler, F. Yen, A. Litvinchuk, and M. Iliev, *Phys. Rev. B* **71**, 172301 (2005).
- <sup>21</sup> A. F. García-Flores, E. Granado, H. Martinho, R. R. Urbano, C. Rettori, E. I. Golovenchits, V. A. Sanina, S. B. Oseroff, S. Park, and S.-W. Cheong, *Phys. Rev. B* **73**, 104411 (2006).
- <sup>22</sup> J. Alonso, M. Casais, M. Martínez-Lope, J. Martínez, and M. Fernández-Díaz, *J. Phys. Condens. Matter* **9**, 8515 (1997).
- <sup>23</sup> H. Katsura, A. V. Balatsky, and N. Nagaosa (2006), Cond-Mat/0602547.
- <sup>24</sup> A. B. Sushkov, R. Valdés Aguilar, S.-W. Cheong, S. Park, and H. D. Drew, to be published.
- <sup>25</sup> E. I. Golovenchits, V. A. Sanin, and A. V. Babinskii, *JETP* **85**, 156 (1997).
- <sup>26</sup> M. J. P. Gingras, B. C. den Hertog, M. Faucher, J. S. Gardner, S. R. Dunsiger, L. J. Chang, B. D. Gaulin, N. P. Raju, and J. E. Greedan, *Phys. Rev. B* **62**, 6496 (2000).
- <sup>27</sup> S. Jandl, private communication (2006).